





Cite this: *Phys. Chem. Chem. Phys.*,
2021, 23, 10274

Imidazole-graphyne: a new 2D carbon nitride with a direct bandgap and strong IR refraction†

Wenyang Zhou,^{abc} Yaguang Guo,^{ab} Yiheng Shen,^{ab} Qian Wang ^{*ab} and
Puru Jena ^{*c}

Six-membered rings are common building blocks of many carbon structures. Recent studies have shown that penta-graphene composed of five-membered carbon rings have properties very different from that of graphene. This has motivated the search for new carbon structures. Among this is cp-graphyne, composed of carbon pentagons and bridged by acetylenic linkers. However, the bandgap of cp-graphyne, like that of graphene, is zero, making it unsuitable for applications in electronics. Herein, we show that a new two-dimensional (2D) carbon nitride structure formed by assembling the five-membered imidazole molecules with acetylenic linker can overcome this limitation. Named ID-GY, this new material not only has a direct band gap of 1.10 eV, but it is dynamically and mechanically stable and can withstand temperatures up to 1200 K. In addition, due to its porous and anisotropic geometry, the Young's modulus of ID-GY along the diagonal direction is lower than that of most 2D materials reported previously. Equally important, ID-GY exhibits strong refraction near infrared (IR) and has potential for applications in nanoelectronics and optical devices. These results, based on density functional theory, can stimulate experimental studies.

Received 21st February 2021,
Accepted 15th April 2021

DOI: 10.1039/d1cp00800e

rsc.li/pccp

Introduction

Carbon, one of the most versatile elements, has various hybridization states (sp, sp² and sp³), which allow diverse covalent bonding between C atoms to form numerous carbon allotropes.¹ In addition to the well-known graphite and diamond, many novel carbon allotropes have been discovered, such as fullerene,² carbon nanotube,³ graphene⁴ and graphyne.⁵ The basic building block of these materials is the 6-membered ring, which makes it possible to directly synthesize them by using benzene as the precursor.^{6,7} As we know, the structure determines the properties. In recent years, more and more evidences showed that 5-membered ring is another important structural unit in a series of carbon nanostructures, such as C₂₀,⁸ penta-graphene,⁹ penta-graphene nanotube^{10,11} and penta-diamond.¹² They exhibit unique properties different from those of the hexagon-based carbon structures. For instance, penta-graphene not only possesses an unusual negative Poisson's ratio, but also has a fundamental quasi-direct band gap of 3.25 eV. In contrast to graphene, which has a zero

band-gap⁹ and needs to be functionalized for applications, penta-graphene can be directly incorporated in electronics in its pristine form.

Among the 2D carbon materials, graphyne possesses a unique structure with sp hybridized $-C\equiv C-$ bonds, hence leading to many special properties that are different from graphene.^{13–15} As a result, graphyne has attracted a lot of attention due to its practical applications. For example, the pore size of graphyne is 5.96 Å, which is two times larger than that of graphene (2.84 Å), thus making it a promising anode material in lithium ion battery¹⁶ and water purification.^{17,18} In addition, graphyne-based nanotubes,¹⁹ nanowalls,²⁰ and nanowires²¹ also have a wide range of applications, exhibiting potential in field emission,²⁰ gas separation,²² catalysis,^{23,24} and solar cells.^{25,26} Consequently, there has been a lot of interest in studying graphyne derivatives and their potentials in technical applications. For example, BN-graphyne²⁷ can provide more flexibility for electronic band engineering; N-graphdiyne²⁸ has low thermal conductivity and high stretchability,²⁸ and 3D phosphorus-graphdiyne²⁹ can be used as anode material for both K- and Ca-ion batteries with an ultra-high specific capacity. However, the basic unit of the above-mentioned structures is still the 6-membered ring. In order to expand graphyne family from hexagon-based to pentagon-based, cp-graphyne was proposed³⁰ where the 6-membered carbon rings are replaced with 5-membered carbon rings, exhibiting a semimetallic nature and possessing double distorted Dirac points. The zero band gap of cp-graphyne results in

^a Center for Applied Physics and Technology, HEDPS, College of Engineering, Peking University, Beijing, 100871, China. E-mail: qianwang2@pku.edu.cn

^b School of Materials Science and Engineering, BKL-MEMD, Peking University, Beijing, 100871, China

^c Department of Physics, Virginia Commonwealth University, Richmond, VA, 23284, USA. E-mail: pjena@vcu.edu

† Electronic supplementary information (ESI) available. See DOI: 10.1039/d1cp00800e

its metallic behavior, while in many applications like photo-voltaics, light-emitting diodes, and laser diodes, materials with semiconducting characteristics, especially those with direct bandgaps, are needed. A question arises: can we design a pentagon-based derivative of graphyne with a direct bandgap by using a 5-membered ring molecule as the precursor?

In this work, we propose a 2D carbon nitride structure, ID-GY, by assembling experimentally synthesized pentagonal imidazole molecule and acetylenic linkers. Imidazole ($C_3N_2H_4$) is a planar 5-membered organic molecule and has non-adjacent N atoms, which belongs to an aromatic heterocycle.^{31–34} Its derivants share the common 1,3- C_3N_2 ring that are important building blocks in biomolecules and drugs such as histidine, histamine and midazolam.^{35–37} Here, we demonstrate that 1, 3- C_3N_2 ring can also form a stable 2D sheet with intriguing electronic and optical properties, going beyond what has been reported previously.

Computational methods

Our calculations are performed using the density functional theory (DFT) and the Vienna *Ab initio* Simulation Package (VASP).^{38,39} Projector-augmented wave (PAW) approach is used to describe the interaction between valence electrons and ions.⁴⁰ Plane waves with a kinetic energy cutoff of 520 eV are adopted to expand the wavefunctions of valence electrons. The exchange–correlation interaction is treated by using the Perdew–Burke–Ernzerhof (PBE) functional within the general gradient approximation (GGA).⁴¹ For more accurate electronic structure calculations, we have used the Heyd–Scuseria–Ernzerhof (HSE06) functional.^{42,43} For structure relaxation and self-consistent calculations we have used $3 \times 3 \times 1$ and $6 \times 6 \times 1$ Monkhorst–Pack k -mesh points, respectively, in the first Brillouin zone.⁴⁴ A vacuum space of 20 Å along the c axis is used to avoid interactions between neighbouring layers. For geometry relaxation, the convergence thresholds of total energy and atomic force are set to 10^{-8} eV and 10^{-6} eV Å⁻¹, respectively. In *ab initio* molecular dynamics (AIMD) simulations, the threshold for total energy is set as 10^{-4} eV, and temperature is controlled by the Nosé–Hoover thermostat.⁴⁵ Phonon spectrum

is calculated by using density functional perturbation theory (DFPT) as implemented in Phonopy code.⁴⁶

Results and discussion

Atomic configuration

Imidazole ($C_3N_2H_4$) is a planar 5-membered ring with three non-equivalent sites after dehydrogenation, labeled C1, C2 and N in Fig. 1. This leads to three different ways of assembling the imidazole molecules with acetylenic linkers. Thus, we generate three configurations, marked I, II, III, as shown in Fig. S1 in the ESI.† The symmetry of configuration I is $P4/mbm$ with the space group of No. 127, which is higher than $P4/m$ with space group of No. 83 for both configuration II and III. Its relative energy is 0.48 and 1.09 eV lower than that of configuration II and III, respectively, suggesting that configuration I with higher symmetry is the energetically favorable structure. Therefore, we focus on this configuration in the following study. Fig. 1(a) shows the optimized structure, where the 5-membered imidazoles are first dehydrogenated and then connected by the acetylenic linkers. Hence, we name it imidazole-graphyne (ID-GY), which forms a tetragonal lattice with $P4/mbm$ ($D4h5$) symmetry. The equilibrium lattice parameters of the unit cell are $a = b = 12.14$ Å. There are 40 atoms in the unit cell containing 8 nitrogen (N) and 32 carbon (C) atoms.

The carbon bonds in ID-GY exhibit slightly altered bond lengths and bond angles from the standard sp and sp² bond parameters in graphene and graphynes.¹³ The calculated C–C and C–N bond lengths are in the range of 1.23–1.41 Å and 1.33–1.43 Å, respectively. The bond lengths around the five-membered rings are all larger than that along the acetylenic linker, as listed in Table 1. In this structure, the central acetylenic type C–C bond is the shortest one (1.23 Å) among all of the C–C and C–N bonds, and the bond angles are in the range of 107–109° and 121–131° in the interior and exterior of the imidazole pentagon, respectively. Some of the acetylenic linkers are slightly distorted from the linear structure with a bond angle of $\sim 167^\circ$. As shown in Fig. 1(b), the charge density is mainly distributed on the N atoms and followed by the C–C bond in acetylenic linker, which is different from that of

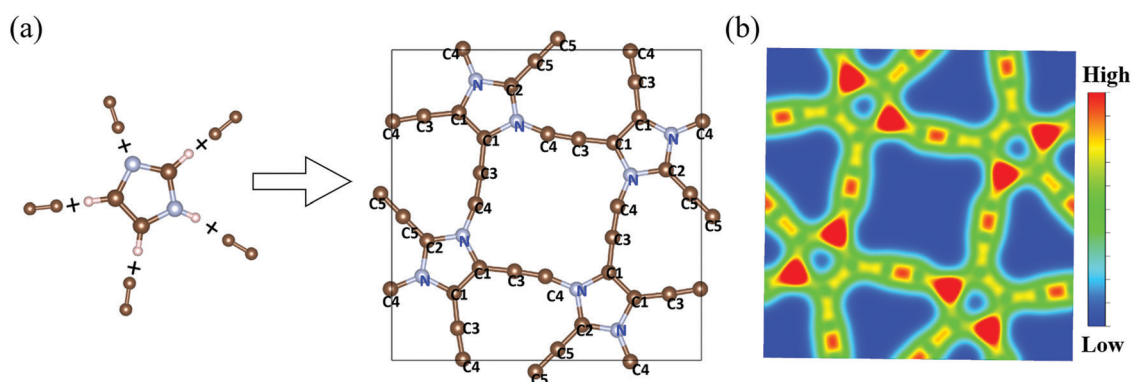


Fig. 1 (a) Optimized geometry of ID-GY and (b) 2D contour plot of the electronic charge density. Brown, blue and pink spheres represent C, N and H atoms, respectively.

Table 1 Geometrical parameters of ID-GY

Geometrical parameters					
Bond length (Å)			Band angles (deg)		
In imidazole pentagon	C1–C1	1.41	Interior of imidazole pentagon	C1–C1–N	107.46
	C1–N	1.43		C1–N–C2	109.00
	C2–N	1.41		N–C2–N	107.08
Along the acetylenic-type linker	C1–C3	1.38	Exterior of imidazole pentagon	C1–C1–C3	129.08
	C2–C5	1.34		C1–N–C4	130.08
	C3–C4	1.23		C2–N–C4	120.91
	C4–N	1.33		C3–C1–N	123.45
	C5–C5	1.24		C5–C2–N	126.46
			Along the acetylenic-type linker	C1–C3–C4	176.48
				C2–C5–C5	180.00
				C3–C4–N	167.06

cp-graphyne where the charge density is mainly accumulated on the acetylenic linker.³⁰ The Wyckoff positions of the five nonequivalent C and N atoms of ID-GY are presented in the Fig. S2 (ESI[†]).

Stability

Dynamic stability. We first study the dynamic stability of ID-GY by calculating its phonon dispersion. A $2 \times 2 \times 1$ supercell is used to calculate the vibrational modes of ID-GY along the high symmetry k -points throughout the first Brillouin zone. The result is presented in Fig. 2(a). No imaginary modes in the first Brillouin zone are found, confirming the dynamical stability of ID-GY. The partial phonon density of states (PhDOS) are also plotted in Fig. 2(a), which shows that the low frequency modes are mainly contributed from C atoms, while N atoms make small contributions. The high frequency modes are only contributed by the C atoms because C is lighter than N in mass. For better visualization of the phonon spectrum, the low frequency region from 0 to 5 THz is amplified in Fig. 2(b). One can see that the ZA branch has parabolic dispersion, while the transverse acoustic (TA) and longitudinal acoustic (LA) branches have linear dispersion, showing the typical feature of 2D materials. In general, for a flat 2D structure with mirror symmetry, the out-of-plane transverse acoustic (ZA) mode

contributes most to the lattice thermal conductivity. For ID-GY, the ZA branch has a small slope, corresponding to a low phonon group velocity, which would lead to a low lattice thermal conductivity in ID-GY.

Thermal stability. Next, we study the thermal stability of ID-GY by performing *ab initio* molecular dynamics (AIMD) simulations. After heating at room temperature (300 K) and then at 1200 K for 10 ps with a time step of 1 fs, we do not observe any obvious structural distortion. The total energy fluctuates around a constant value throughout the simulation range, as shown in Fig. 2(b). The snapshots of atomic configurations at the end of simulation are also depicted in Fig. 2(b). One can see that the C atoms in acetylenic linkers remain almost intact. Therefore, we conclude that ID-GY is thermally stable and can withstand a temperature as high as 1200 K.

Mechanical stability. The mechanical stability of ID-GY was examined by evaluating the independent elastic stiffness tensor components. In the linear elastic range, the elastic constant tensor forms a symmetric 6×6 matrix with 21 independent components. For this 2D lattice, only C_{11} , C_{12} and C_{66} are non-zero and independent due to the lattice symmetry. The calculated elastic constants are $C_{11} = C_{22} = 161.12 \text{ N m}^{-1}$, $C_{12} = 84.93 \text{ N m}^{-1}$ and $C_{66} = 12.62 \text{ N m}^{-1}$. According to the Born criteria,⁴⁷ this stable 2D sheet should satisfy the following

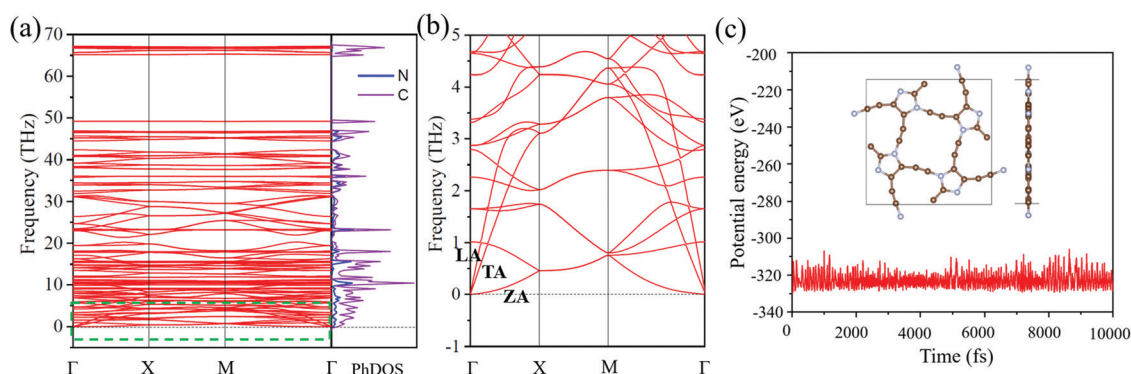


Fig. 2 (a) Phonon spectrum and PhDOS, and (b) phonon spectrum of the low frequency region from 0 to 5 THz, and (c) total potential energy fluctuation of ID-GY during AIMD simulation at 1200 K. The insets show the snapshot at the end of simulation.

conditions: $C_{11}C_{22} - C_{12}^2 > 0$, $C_{66} > 0$. Note that above conditions are fully satisfied, indicating that 2D ID-GY sheet is also mechanically stable.

Properties

Mechanical properties. The mechanical behavior of ID-GY is explored by calculating the in-plane Young's modulus $Y(\theta)$ and Poisson's ratio $\nu(\theta)$ on the basis of the calculated elastic constants. $Y(\theta)$ and $\nu(\theta)$ along the in-plane direction θ can be expressed as follows:

$$Y(\theta) = \frac{C_{11}C_{22} - C_{12}^2}{C_{11}\sin^4\theta + A\sin^2\theta\cos^2\theta + C_{22}\cos^4\theta} \quad (1)$$

$$\nu(\theta) = \frac{C_{12}\sin^4\theta - B\sin^2\theta\cos^2\theta + C_{12}\cos^4\theta}{C_{11}\sin^4\theta + A\sin^2\theta\cos^2\theta + C_{22}\cos^4\theta} \quad (2)$$

where $A = (C_{11}C_{22} - C_{12}^2)/(C_{66} - 2C_{12})$, and $B = (C_{11} + C_{22} - (C_{11}C_{22} - C_{12}^2))/C_{66}$.

Young's modulus reflects the flexibility or rigidity of a material, and a flexible material usually has a low Young's modulus. Because of the anisotropic structure, the Young's modulus $Y(\theta)$ of ID-GY exhibits strong anisotropy as shown in Fig. 3(a), which reaches its highest value of 116 N m^{-1} along the axial direction, while it becomes 46 N m^{-1} along the diagonal direction. This suggests that ID-GY has moderate rigidity against deformation along the axial direction, but it is soft along the diagonal direction. When compared with other 2D sheets, the Young's modulus of ID-GY is relatively smaller than that of graphene (1000 N m^{-1}),⁴⁸ MoS₂ (330 N m^{-1})⁴⁹ and synthesized C₃N (340 N m^{-1}).⁵⁰

Poisson's ratio is defined as the ratio of the strain in the transverse direction to that of the longitudinal direction. This reflects the mechanical response of the system against uniaxial strain. As plotted in Fig. 3(b), the Poisson's ratio reaches its maximum of 0.81 along the axial direction, while the minimum value is 0.53 along the diagonal direction, which also confirms the mechanical anisotropy of ID-GY.

Electronic properties. To investigate the electronic properties of 2D ID-GY, we calculate its band structure and the corresponding total and partial density of states (DOS). As shown in

Fig. 4, ID-GY is a direct band-gap semiconductor with a band gap of 1.10 eV at the HSE06 level, different from the zero band gap of cp-graphyne that has double Dirac points in the first Brillouin zone.³⁰ Analysis of total and partial DOS reveals that the electronic states near the Fermi level mainly originate from the contribution of N and C2 atoms, which is further confirmed by calculating the band-decomposed charge density distributions, as shown in Fig. 4(e) and (f).

Optical properties. Finally, we study the optical properties of ID-GY. The frequency-dependent complex dielectric function $\varepsilon(\omega) = \varepsilon_1(\omega) + i\varepsilon_2(\omega)$ of a material is closely related to its electronic band structure, and the real part $\varepsilon_1(\omega)$ and imaginary part $\varepsilon_2(\omega)$ can be described by the following equations

$$\varepsilon_2(\omega) = \frac{4}{\pi\omega^2} \sum_{m'} \int |P_{mm'}(k)|^2 \frac{dS_k}{\nabla\omega_{mm'}(k)} \quad (3)$$

and

$$\varepsilon_1(\omega) = 1 + \frac{2}{\pi} P \int_0^\infty \frac{\omega' \varepsilon_2(\omega')}{\omega'^2 - \omega^2} d\omega' \quad (4)$$

All linear optical properties such as the absorption coefficient, $I(\omega)$, the refraction index, $n(\omega)$, and the reflectivity, $R(\omega)$ can be deduced from $\varepsilon(\omega)$ ⁵¹ as shown below:

$$I(\omega) = \sqrt{2}\omega \left[\sqrt{\varepsilon_1(\omega)^2 + \varepsilon_2(\omega)^2} - \varepsilon_1(\omega) \right]^{\frac{1}{2}} \quad (5)$$

$$n(\omega) = \frac{\sqrt{2}}{2} \left[\sqrt{\varepsilon_1(\omega)^2 + \varepsilon_2(\omega)^2} + \varepsilon_1(\omega) \right]^{\frac{1}{2}} \quad (6)$$

$$R(\omega) = \left| \frac{\varepsilon(\omega)^{1/2} - 1}{\varepsilon(\omega)^{1/2} + 1} \right|^2 \quad (7)$$

According to above equations, the peaks of $\varepsilon_1(\omega)$ and $\varepsilon_2(\omega)$ are found to be at 1.10 and 1.25 eV, respectively. $\varepsilon_2(\omega)$ has negligible values for photons with energy less than ~ 1 eV, indicating that few dipole transitions can occur under such stimulation, which agrees well with the band gap of ID-GY. As for the absorption coefficient in Fig. 5(b),

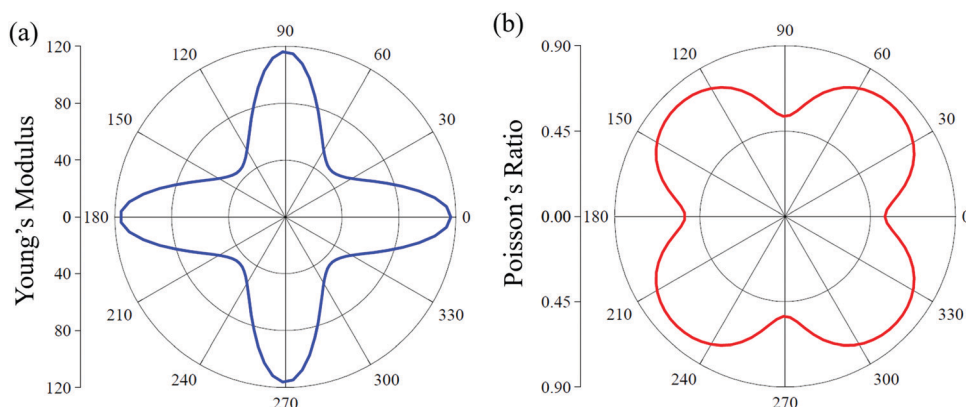


Fig. 3 (a) Young's modulus and (b) Poisson's ratio of ID-GY as a function of the angle θ . $\theta = 0^\circ$ corresponds to the x-axis.

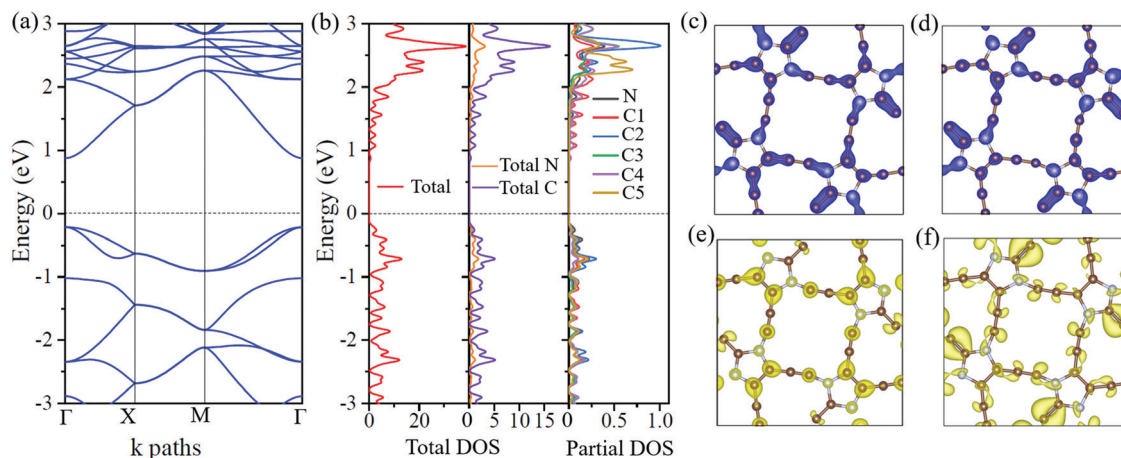


Fig. 4 (a) Electronic band structure and (b) corresponding total and partial DOS, (c) the second highest occupied band, (d) the highest occupied band, (e) the lowest unoccupied band, and (f) the second lowest unoccupied band of 2D ID-GY.

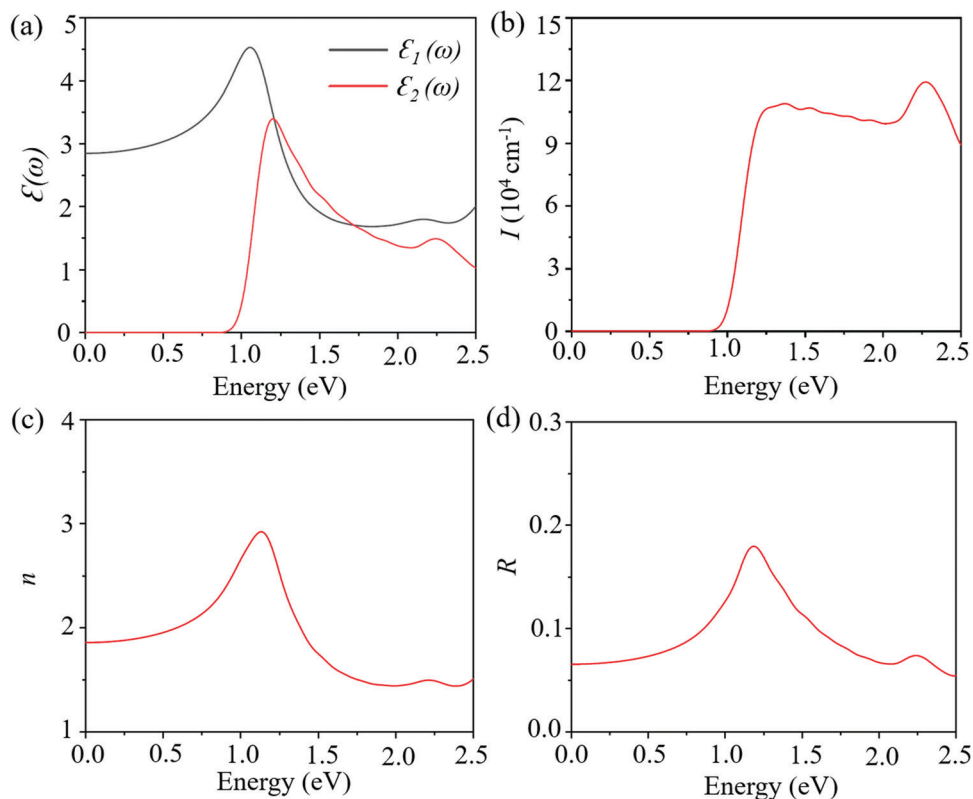


Fig. 5 (a) Optical absorption $\varepsilon_1(\omega)$ and $\varepsilon_2(\omega)$, (b) absorption coefficient I , (c) refractive index n and (d) reflectivity R of ID-GY.

ID-GY exhibits a moderate adsorption with the 10^5 cm^{-1} order of magnitude in the energy range of the visible light, which has almost the same order as that of cp-graphyne (see Fig. S3, ESI†). The curve of refractive index has less fluctuation when the energy is above 1.7 eV, as shown in Fig. 5(c). This implies that the dispersion to light with different wavelengths in that range is small. One can also see from Fig. 5(c) that ID-GY has large refractive index up to

3 in the near-infrared spectra, which is higher than that of ruby (1.77) and glass (1.5–1.9), and is comparable to that of diamond (2.42). As shown in Fig. 5(d), there is a peak at 1.2 eV in the incident light spectrum, corresponding to the climax (about 20%) of the overall reflectivity. The strong refraction and reflection in the near-infrared spectra indicate that ID-GY could have potential applications in optical splitter and lens.

Conclusions

Precursor-based bottom-up approach has been widely used for the synthesis of graphene sheet and other 2D materials. In this work, we have proposed a new 2D carbon nitride material, ID-GY, which can be assembled from imidazole molecules with acetylenic linkers. Based on systematic theoretical calculations, the following conclusions can be made: (1) ID-GY is not only mechanically and dynamically stable, but also can withstand temperatures as high as 1200 K. (2) It exhibits $P4/mbm$ symmetry and has anisotropic mechanical properties. (3) Its Young's modulus along the diagonal direction, namely 46 N m^{-1} , is lower than that of most 2D materials reported previously. (4) Unlike cp-graphyne that needs to be functionalized for opening a band gap, ID-GY is a direct band-gap semiconductor. With a band gap of 1.10 eV, and strong refraction and reflection in the near-infrared spectra, ID-GY has the potential for applications in nanoelectronics and optical devices. Our study expands the family of graphyne derivative with new features and is expected to stimulate experimental synthesis and further investigations.

Conflicts of interest

There are no conflicts to declare.

Acknowledgements

This work is partially supported by grants from the National Key Research and Development Program of the Ministry of Science and Technology of China (2017YFA0205003), and National Natural Science Foundation of China (NSFC-11974028 and NSFC-21773004) and is supported by the High Performance Computing Platform of Peking University, China. P. J. acknowledges partial support by the U.S DOE, Office of Basic Energy Sciences, Division of Material Sciences and Engineering under Award No. DE-FG02-96ER45579. W. Z. acknowledges the China Scholarship Council (CSC) for sponsoring his visit to Virginia Commonwealth University (VCU), where the present work is partially conducted.

References

- 1 A. Hirsch, *Nat. Mater.*, 2010, **9**, 868–871.
- 2 H. W. Kroto, J. R. Heath, S. C. O'Brien, R. F. Curl and R. E. Smalley, *Nature*, 1985, **318**, 162–163.
- 3 S. Iijima, *Nature*, 1991, **354**, 56–58.
- 4 K. S. Novoselov, A. K. Geim, S. V. Morozov, D. Jiang, Y. Zhang, S. V. Dubonos, I. V. Grigorieva and A. A. Firsov, *Science*, 2004, **306**, 666.
- 5 Y. Li, L. Xu, H. Liu and Y. Li, *Chem. Soc. Rev.*, 2014, **43**, 2572–2586.
- 6 L. C. Lopes, L. C. da Silva, B. G. Vaz, A. R. M. Oliveira, M. M. Oliveira, M. L. M. Rocco, E. S. Orth and A. J. G. Zarbin, *Chem. Sci.*, 2018, **9**, 7297–7303.
- 7 Q. Li, C. Yang, L. Wu, H. Wang and X. Cui, *J. Mater. Chem. A*, 2019, **7**, 5981–5990.
- 8 H. Prinzbach, A. Weiler, P. Landenberger, F. Wahl, J. Wörth, L. T. Scott, M. Gelmont, D. Olevano and B. V. Issendorff, *Nature*, 2000, **407**, 60–63.
- 9 S. Zhang, J. Zhou, Q. Wang, X. Chen, Y. Kawazoe and P. Jena, *Proc. Natl. Acad. Sci. U. S. A.*, 2015, **112**, 2372.
- 10 M. Chen, H. Zhan, Y. Zhu, H. Wu and Y. Gu, *J. Phys. Chem. C*, 2017, **121**, 9642–9647.
- 11 Z. Wang, X. Cao, C. Qiao, R. J. Zhang, Y. X. Zheng, L. Y. Chen, S. Y. Wang, C. Z. Wang, K. M. Ho, Y.-J. Fan, B.-Y. Jin and W.-S. Su, *Nanoscale*, 2017, **9**, 19310–19317.
- 12 Y. Fujii, M. Maruyama, N. T. Cuong and S. Okada, *Phys. Rev. Lett.*, 2020, **125**, 016001.
- 13 R. H. Baughman, H. Eckhardt and M. Kertesz, *J. Chem. Phys.*, 1987, **87**, 6687–6699.
- 14 J. Kang, Z. Wei and J. Li, *ACS Appl. Mater. Interfaces*, 2019, **11**, 2692–2706.
- 15 G. Li, Y. Li, H. Liu, Y. Guo, Y. Li and D. Zhu, *Chem. Commun.*, 2010, **46**, 3256–3258.
- 16 H. Zhang, M. Zhao, X. He, Z. Wang, X. Zhang and X. Liu, *J. Phys. Chem. C*, 2011, **115**, 8845–8850.
- 17 X. Gao, J. Zhou, R. Du, Z. Xie, S. Deng, R. Liu, Z. Liu and J. Zhang, *Adv. Mater.*, 2016, **28**, 168–173.
- 18 R. Liu, J. Zhou, X. Gao, J. Li, Z. Xie, Z. Li, S. Zhang, L. Tong, J. Zhang and Z. Liu, *Adv. Electron. Mater.*, 2017, **3**, 1700122.
- 19 G. Li, Y. Li, X. Qian, H. Liu, H. Lin, N. Chen and Y. Li, *J. Phys. Chem. C*, 2011, **115**, 2611–2615.
- 20 J. Zhou, X. Gao, R. Liu, Z. Xie, J. Yang, S. Zhang, G. Zhang, H. Liu, Y. Li, J. Zhang and Z. Liu, *J. Am. Chem. Soc.*, 2015, **137**, 7596–7599.
- 21 X. Qian, Z. Ning, Y. Li, H. Liu, C. Ouyang, Q. Chen and Y. Li, *Dalton Trans.*, 2012, **41**, 730–733.
- 22 Z. Meng, X. Zhang, Y. Zhang, H. Gao, Y. Wang, Q. Shi, D. Rao, Y. Liu, K. Deng and R. Lu, *ACS Appl. Mater. Interfaces*, 2016, **8**, 28166–28170.
- 23 S. Wang, L. Yi, J. E. Halpert, X. Lai, Y. Liu, H. Cao, R. Yu, D. Wang and Y. Li, *Small*, 2012, **8**, 265–271.
- 24 J. Li, X. Gao, B. Liu, Q. Feng, X.-B. Li, M.-Y. Huang, Z. Liu, J. Zhang, C.-H. Tung and L.-Z. Wu, *J. Am. Chem. Soc.*, 2016, **138**, 3954–3957.
- 25 C. Kuang, G. Tang, T. Jiu, H. Yang, H. Liu, B. Li, W. Luo, X. Li, W. Zhang, F. Lu, J. Fang and Y. Li, *Nano Lett.*, 2015, **15**, 2756–2762.
- 26 J. Xiao, J. Shi, H. Liu, Y. Xu, S. Lv, Y. Luo, D. Li, Q. Meng and Y. Li, *Adv. Energy Mater.*, 2015, **5**, 1401943.
- 27 J. Zhou, K. Lv, Q. Wang, X. S. Chen, Q. Sun and P. Jena, *J. Chem. Phys.*, 2011, **134**, 174701.
- 28 B. Mortazavi, M. Makaremi, M. Shahrokhi, Z. Fan and T. Rabczuk, *Carbon*, 2018, **137**, 57–67.
- 29 I. Muhammad, U. Younis, W. Wu, H. Xie, A. Khaliq and Q. Sun, *J. Power Sources*, 2020, **480**, 228876.
- 30 N. V. R. Nulakani and V. Subramanian, *ACS Omega*, 2017, **2**, 6822–6830.
- 31 H. Debus, *Justus Liebigs Ann. Chem.*, 1858, **107**, 199–208.
- 32 Y. Segawa, M. Yamashita and K. Nozaki, *Science*, 2006, **314**, 113.

- 33 H. W. Wanzlick, *Angew. Chem., Int. Ed. Engl.*, 1962, **1**, 75–80.
- 34 B. Borthakur, B. Silvi, R. D. Dewhurst and A. K. Phukan, *J. Comput. Chem.*, 2016, **37**, 1484–1490.
- 35 A. R. Katritzky and C. W. Rees, *Comprehensive heterocyclic chemistry*, Pergamon Press, 1984.
- 36 K. Shalini, P. K. Sharma and N. J. D. C. S. Kumar, *Der Chemica Sinica*, 2010, **1**, 36–47.
- 37 E. J. H. Brown, *Ring nitrogen and key biomolecules: The biochemistry of N-heterocycles*, Kluwer Academic Publishers, The Netherlands, 1998.
- 38 G. Kresse and J. Furthmuller, *Phys. Rev. B: Condens. Matter Mater. Phys.*, 1996, **54**, 11169–11186.
- 39 G. Kresse and J. Furthmuller, *Comput. Mater. Sci.*, 1996, **6**, 15–50.
- 40 P. E. Blöchl, *Phys. Rev. B: Condens. Matter Mater. Phys.*, 1994, **50**, 17953.
- 41 J. P. Perdew, K. Burke and M. Ernzerhof, *Phys. Rev. Lett.*, 1996, **77**, 3865.
- 42 J. Heyd, G. E. Scuseria and M. Ernzerhof, *J. Chem. Phys.*, 2003, **118**, 8207–8215.
- 43 J. Heyd, G. E. Scuseria and M. Ernzerhof, *J. Chem. Phys.*, 2006, **124**, 219906.
- 44 H. J. Monkhorst and J. D. Pack, *Phys. Rev. B: Condens. Matter Mater. Phys.*, 1976, **13**, 5188–5192.
- 45 S. Nosé, *J. Chem. Phys.*, 1984, **81**, 511–519.
- 46 S. Baroni, S. de Gironcoli, A. Dal Corso and P. Giannozzi, *Rev. Mod. Phys.*, 2001, **73**, 515–562.
- 47 M. Born and K. Huang, *Dynamical theory of crystal lattices*, Clarendon press, 1954.
- 48 C. Lee, X. Wei, J. W. Kysar and J. Hone, *Science*, 2008, **321**, 385.
- 49 A. Castellanos-Gomez, M. Poot, G. A. Steele, H. S. Van Der Zant, N. Agrait and G. J. A. M. Rubio-Bollinger, *Adv. Mater.*, 2012, **24**, 772–775.
- 50 B. Mortazavi, *Carbon*, 2017, **118**, 25–34.
- 51 Y. Li, X. Zhao and W. Fan, *J. Phys. Chem. C*, 2011, **115**, 3552–3557.